

## Effect of indium content on X- ray diffraction and optical constants of $In_xSe_{1-x}$ thin films

Bushra A. Hasan, Iyat M. Abdulrazzaq

Department of Physics, College of Science, University of Baghdad

E-mail: Bushra\_abhasan@yahoo.com

### Abstract

Alloys of  $In_xSe_{1-x}$  were prepared by quenching technique with different In content ( $x=10, 20, 30,$  and  $40$ ). Thin films of these alloys were prepared using thermal evaporation technique under vacuum of  $10^{-5}$  mbar on glass, at room temperature R.T with different thicknesses ( $t=300, 500$  and  $700$  nm). The X-ray diffraction measurement for bulk  $In_xSe_{1-x}$  showed that all alloys have polycrystalline structures and the peaks for  $x=10$  identical with Se, while for  $x=20, 30$  and  $40$  were identical with the Se and InSe standard peaks. The diffraction patterns of  $In_xSe_{1-x}$  thin film show that with low In content ( $x=10,$  and  $20$ ) samples have semi crystalline structure, The increase of indium content to  $x=30$  decreases degree of crystallinity and further increase of indium content to  $x=40$  leads to convert structure to amorphous. Increase of thickness from  $300$  to  $700$ nm increases degree of crystallinity for all indium content. Transmittance measurements were used to calculate refractive index  $n$  and the extinction coefficient  $k$  using Swanepole's method. The optical constants such as refractive index ( $n$ ), extinction coefficient ( $k$ ) and dielectric constant ( $\epsilon_r, \epsilon_i$ ) increases for low indium content samples and decreases for high indium content samples, while increase of thickness increases optical constants for all  $x$  values. The oscillator energy  $E_0$ , dispersion energy  $E_d$ , and other parameters have been determined by Wemple - DiDomenico single oscillator approach.

### Key words

$In_xSe_{1-x}$  thin films, Refractive index, Oscillator energy, Dispersion energy, X-ray diffraction.

### Article info.

Received: Sep. 2015

Accepted: Nov. 2015

Published: Apr. 2016

### تأثير حيود الانديوم على حيود الاشعة السينية و الثوابت البصرية لاغشية $In_xSe_{1-x}$ الرقيقة

بشرى عباس حسن، ايات منير عبد الرزاق

قسم الفيزياء، كلية العلوم، جامعة بغداد

### الخلاصة

تم تحضير سبائك من  $In_xSe_{1-x}$  وبمحتوى مختلف من الانديوم ( $x=10, 20, 30,$  and  $40$ ) باستخدام طريقة الانجماد السريع للمنصهر. حضرت اغشية رقيقة من هذه السبائك باستخدام طريقة التبخير الحراري تحت الفراغ  $10^{-5}$  mbar على قواعد زجاجية عند درجة حرارة الغرفة باسماك مختلفة ( $t=300, 500, 700$ ) نانوميتر. اظهر فحص الاشعة السينية ان سبائك  $In_xSe_{1-x}$  كانت متعددة البلورات وان القمة عند  $x=10$  كانت متطابقة مع قمم Se القياسية بينما كانت متطابقة مع قمم Se و InSe القياسية لقيم  $x=20, 30$  و  $40$ . اظهر طيف الاشعة السينية لاغشية  $In_xSe_{1-x}$  الرقيقة ان النماذج ذات المحتوى الواطيء من الانديوم  $20$  و  $x=10$  كانت ذات تركيب شبه بلوري. زيادة المحتوى من الانديوم الى  $x=30$  يقلل درجة التبلور وان الزيادة اكثر الى  $x=40$  يؤدي الى تحويل التركيب الى عشوائي. زيادة السمك من  $300$  الى  $700$  نانوميتر يزيد من درجة التبلور لكل قيم المحتوى من الانديوم. تم حساب الثوابت البصرية وهي معامل الانكسار، معامل الخمود، من قياس طيف النفاذ باستخدام طريقة Swanepole. الثوابت البصرية معامل الانكسار، معامل الخمود، ثابت العزل الحقيقي والخيالي ازدادت للعينات ذات المحتوى الواطيء من الانديوم وقلت للعينات ذات المحتوى العالي من الانديوم، بينما ازدادت الثوابت البصرية مع زيادة السمك لكل قيم المحتوى من الانديوم. تم حساب طاقة التذبذب والتشتيت ومعاملات اخرى من تقريب Wemple - DiDomenico للمتذبذب المنفرد.

## Introduction

Numerous interest have been shown on Indium monoselenide (InSe) is a semiconducting layered compound since it exhibits good photoelectric property and can be used as an active media for the generation of visible and near-infrared radiation[1-14]. Indium selenide (InSe) thin films have been prepared by Hossain et al. [15] using electron-beam evaporation technique onto glass substrate at a pressure of  $\sim 8 \times 10^{-5}$  Pa. Indium selenide thin films have been grown on p-type gallium selenide single crystal substrates using van der Waals epitaxy by Sa'nchez-Royo et al. [16]. The obtained findings and analysis of the experimental and measurements of X-ray diffraction for thin films, optical properties for  $\text{In}_x\text{Se}_{1-x}$  thin films at different In contents ( $x = 10, 20, 30,$  and  $40$ ) and different thicknesses ( $t = 300, 500$  and  $700$  nm) which include optical energy gap as well as optical constants as well the dispersion parameters like, The oscillator energy  $E_0$ , dispersion energy  $E_d$ , static refractive index, and static dielectric constant,  $\epsilon_s$  were also have been measured.

## Experimental procedure

The bulk alloys material was prepared by mixing quantities of high-purity (99.999%) indium and selenium powder in various atomic weight proportions 10/90, 20/80, 30/70, and 40/60. The mixture was sealed in an evacuated quartz tube at pressure  $10^{-5}$  torr and heated at 1073 K for 10 hr in furnace and then quenched in air.  $\text{In}_x\text{Se}_{1-x}$  films have been deposited by thermal evaporation technique under vacuum of about  $10^{-5}$  torr. The substrate to source distance was kept 15cm. The samples of different thicknesses were deposited under similar conditions. The thickness of the films was estimated using the weighting method which provided that

the evaporation was done on half circle. In each deposition, a given quantity of material was taken in the boat of molybdenum and evaporated at the rate of 5 to 10  $\text{A}^\circ$  per second. Before evaporation, the glass substrates were cleaned thoroughly using concentrated chromic acid, detergent, isopropyl alcohol and distilled water. The film thickness was measured by the Tolanasky interference method with an accuracy of  $\pm 10$  nm[9].

X – Ray diffractogram (Rigaku Miniflex, Japan) were obtained of these samples to find out structural information and to identify the film structure qualitatively. The scanning angle ( $2\theta$ ) range was from  $20^\circ - 80^\circ$  (CuK $\alpha$  line). The transmittance was measured by UV-VIS spectrophotometer model no. Shimadzu -2450.

## Results and discussion

Fig.1 shows the X-ray diffraction patterns for bulk ( $\text{In}_x\text{Se}_{1-x}$ ) at different Indium contents ( $x= 10, 20, 30$  and  $40$ ). Table 1 shows a comparison between the experimental and the standard peaks from International Centre for Diffraction Data (JCPDS) for  $\text{In}_{10}\text{Se}_{90}$ ,  $\text{In}_{20}\text{Se}_{80}$ ,  $\text{In}_{30}\text{Se}_{70}$  and  $\text{In}_{40}\text{Se}_{60}$  crystal and their miller indices. The presence of large number of peaks indicates that the films are polycrystalline in nature. It shows that all peaks in the first and second patterns which correspond to  $x= 10$  and 20% In content are identically with the Se standard peaks with hexagonal structures, with preferred plane (011) located at  $2\theta = 29.62^\circ$  for crystal growth, while at  $x=30$  and 40 the preferred plane for crystal growth peaks becomes at  $2\theta = 25.4^\circ$  corresponding to plane (100) which corresponding to InSe phase on the expense of the intensity of Se plane.

The X-ray diffraction (XRD) patterns of alloys are showed the presence of polycrystalline, InSe, along with free Se were detected for all the indium concentration alloys samples suggesting a very stable structure of In-Se. Increasing of indium concentration simply indicated decrease in grain size as. No another intermediate phase such as  $\text{In}_2\text{Se}_3$  or  $\text{In}_2\text{Se}$  has been detected which commonly observed with In-Se materials prepared by vacuum evaporation techniques [15]. The  $\text{In}_2\text{Se}$  phase may arise due to loss of Se deposited at a lower substrate temperature [17] or annealed at a higher temperature. A similar preferred orientation of (110) plane in InSe alloy was observed by Cheon. [18] and by Emziane et al. [19] in the thin films grown by the Vacuum Evaporation Technique and by Emziane et al. [17] prepared method. Whereas Jareeze [20] observed preferred orientation in the (101) while Hossain et al. [15]

indicated that plane of proffered crystal growth was (221). Also Hossain et al [21] in another paper pointed out that plane of proffered crystal growth was (420), According to XRD results, InSe thin films prepared by e-beam technique are polycrystalline hexagonal system with lattice parameters:  $a = 19.20 \text{ \AA}$ ,  $b = 19.20 \text{ \AA}$  and  $c = 4.00 \text{ \AA}$ , respectively. The various preferred orientation reported for InSe films indicate that the deposition technique plays an important role for the orientation of InSe thin film deposition. The XRD data have also found useful for establishing  $d_{hkl}$ , the grain size,  $D$ , can be estimated using the Scherer's formula of the preferential orientation along (100) plane. The average size of crystallites was estimated about 31.5 nm increases little to 32.4 nm with increase of indium concentration to  $x=20$ , followed by decreasing to 23.1nm with further increase of indium concentration, see Table 1.

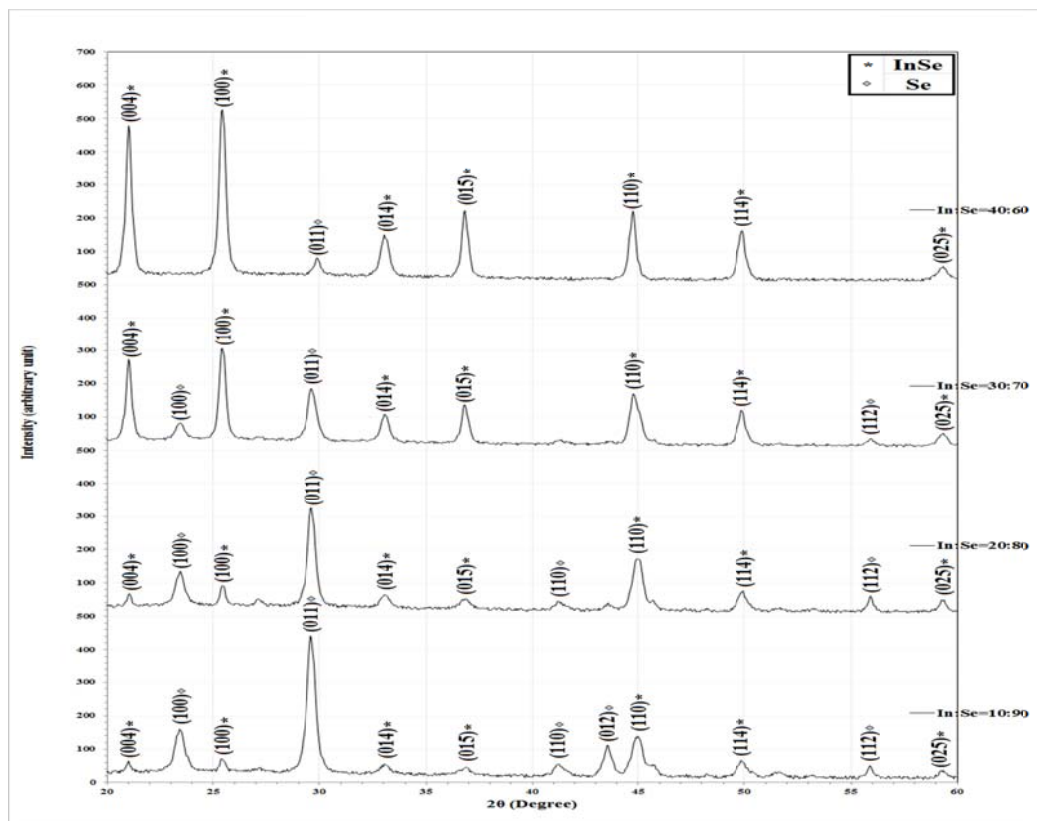


Fig. 1: X-ray diffraction patterns for bulk In:Se at different ratio.

Table 1: Structural parameters for bulk In:Se at different ratio.

In:Se	2 $\theta$ (Deg.)	FWHM (Deg.)	Int. (a.u)	d <sub>hkl</sub> Exp.(Å)	G.S (nm)	hkl	Phase	d <sub>hkl</sub> Std.(Å)	Card No.
10:90	21.010	0.259	27	4.2250	31.2	(004)	InSe	4.2325	900-8968
	23.440	0.518	127	3.7922	15.7	(100)	Se	3.7828	901-1649
	25.430	0.259	40	3.4997	31.5	(100)	InSe	3.5074	900-8968
	29.620	0.471	410	3.0135	17.5	(011)	Se	3.0074	901-1649
	33.060	0.541	26	2.7074	15.3	(014)	InSe	2.7006	900-8968
	36.840	0.606	20	2.4378	13.8	(015)	InSe	2.4361	900-8968
	41.180	0.306	26	2.1904	27.7	(110)	Se	2.1840	901-1649
	43.580	0.465	90	2.0751	18.4	(012)	Se	2.0734	901-1649
	45.000	0.571	110	2.0129	15.1	(110)	InSe	2.0250	900-8968
	49.890	0.476	51	1.8264	18.4	(021)	Se	1.7672	901-1649
	55.880	0.329	33	1.6440	27.3	(112)	Se	1.6387	901-1649
59.300	0.400	20	1.5571	22.9	(025)	InSe	1.5572	900-8968	
20:80	21.022	0.249	35	4.2225	32.5	(004)	InSe	4.2325	900-8968
	23.452	0.466	100	3.7902	17.4	(100)	Se	3.7828	901-1649
	25.442	0.251	60	3.4981	32.4	(100)	InSe	3.5074	900-8968
	29.632	0.424	300	3.0123	19.4	(011)	Se	3.0074	901-1649
	33.072	0.487	35	2.7064	17.0	(014)	InSe	2.7006	900-8968
	36.852	0.545	30	2.4370	15.4	(015)	InSe	2.4361	900-8968
	41.192	0.275	10	2.1897	30.8	(110)	Se	2.1840	901-1649
	45.012	0.514	150	2.0124	16.7	(110)	InSe	2.0250	900-8968
	49.902	0.428	60	1.8260	20.5	(021)	Se	1.7672	901-1649
	55.892	0.296	45	1.6437	30.4	(112)	Se	1.6387	901-1649
	59.312	0.360	36	1.5568	25.4	(025)	InSe	1.5572	900-8968
30:70	20.984	0.313	249	4.2301	25.8	(004)	InSe	4.2325	900-8968
	23.445	0.403	48	3.7913	20.2	(100)	Se	3.7828	901-1649
	25.369	0.358	279	3.5080	22.8	(100)	InSe	3.5074	900-8968
	29.620	0.447	159	3.0136	18.4	(011)	Se	3.0074	901-1649
	33.020	0.447	81	2.7106	18.5	(014)	InSe	2.7006	900-8968
	36.779	0.313	118	2.4417	26.7	(015)	InSe	2.4361	900-8968
	44.743	0.537	151	2.0239	16.0	(110)	InSe	2.025	900-8968
	49.843	0.403	107	1.8280	21.8	(021)	Se	1.7672	901-1649
	55.884	0.358	24	1.6439	25.1	(112)	Se	1.6387	901-1649
	59.329	0.447	35	1.5564	20.4	(025)	InSe	1.5572	900-8968
	40:60	21.010	0.329	450	4.2250	24.6	(004)	InSe	4.2325
25.430		0.353	500	3.4997	23.1	(100)	InSe	3.5074	900-8968
29.920		0.329	50	2.9840	25.0	(011)	Se	3.0074	901-1649
33.060		0.447	120	2.7074	18.5	(014)	InSe	2.7006	900-8968
36.840		0.353	200	2.4378	23.7	(015)	InSe	2.4361	900-8968
44.750		0.353	200	2.0236	24.3	(110)	InSe	2.025	900-8968
49.890		0.400	150	1.8264	21.9	(021)	Se	1.7672	901-1649
59.300		0.541	40	1.5571	16.9	(025)	InSe	1.5572	900-8968

XRD patterns of  $\text{In}_x\text{Se}_{1-x}$  representative films samples with various In concentration are shown in Figs.2-5. Fig.2 depicts that as-deposited  $\text{In}_{10}\text{Se}_{90}$  films with low thickness ( $t=300\text{nm}$ ) begin to crystallize since only one small peak observed at  $2\theta=41.19^\circ$ . The increase of thickness lead to well crystallization of the prepared samples films, which reflects as the increase of peaks numbers at  $2\theta=23.46^\circ$  and  $29.52^\circ$  for  $t=500$ ,  $2\theta=23.46^\circ$ ,  $29.7^\circ$  and  $41.8^\circ$  for  $x=700\text{nm}$  as well as increase the peak intensity.

Fig.3 depicts that as-deposited  $\text{In}_{20}\text{Se}_{80}$  films, similar observation can be given, since samples with low thickness ( $t=300\text{nm}$ ) begin to crystallize, only one small peak observed at  $2\theta=23.44^\circ$ . The increase of thickness lead to well crystallization of the prepared samples films, which reflects the increase of peaks numbers at  $2\theta=23.48^\circ$  and  $29.68^\circ$  for  $t=500$ ,  $2\theta=23.44^\circ$  and

$29.62^\circ$  for  $x=700\text{nm}$  as well as increase the peak intensity.

The interesting result can be observed from Fig.4 for as-deposited  $\text{In}_{30}\text{Se}_{70}$  films is the absent of any diffraction peak which indicate the amorphous nature of the prepared films with low thickness (i.e.  $t=300$  and  $500\text{nm}$ ) begin to crystallize with increase of thickness to  $700\text{nm}$ . The diffraction pattern appear two peak located observed at  $2\theta=23.44^\circ$  and  $41.181^\circ$ . The further increase of In concentration can be observed from diffraction pattern of as-deposited  $\text{In}_{40}\text{Se}_{60}$  films in Fig. 5. The significant result is the absent of any diffraction peak which indicate the amorphous nature of all the prepared films with all thickness.

These figures give indications that increase of thickness has significant effect on the structures of the prepared samples for all indium.

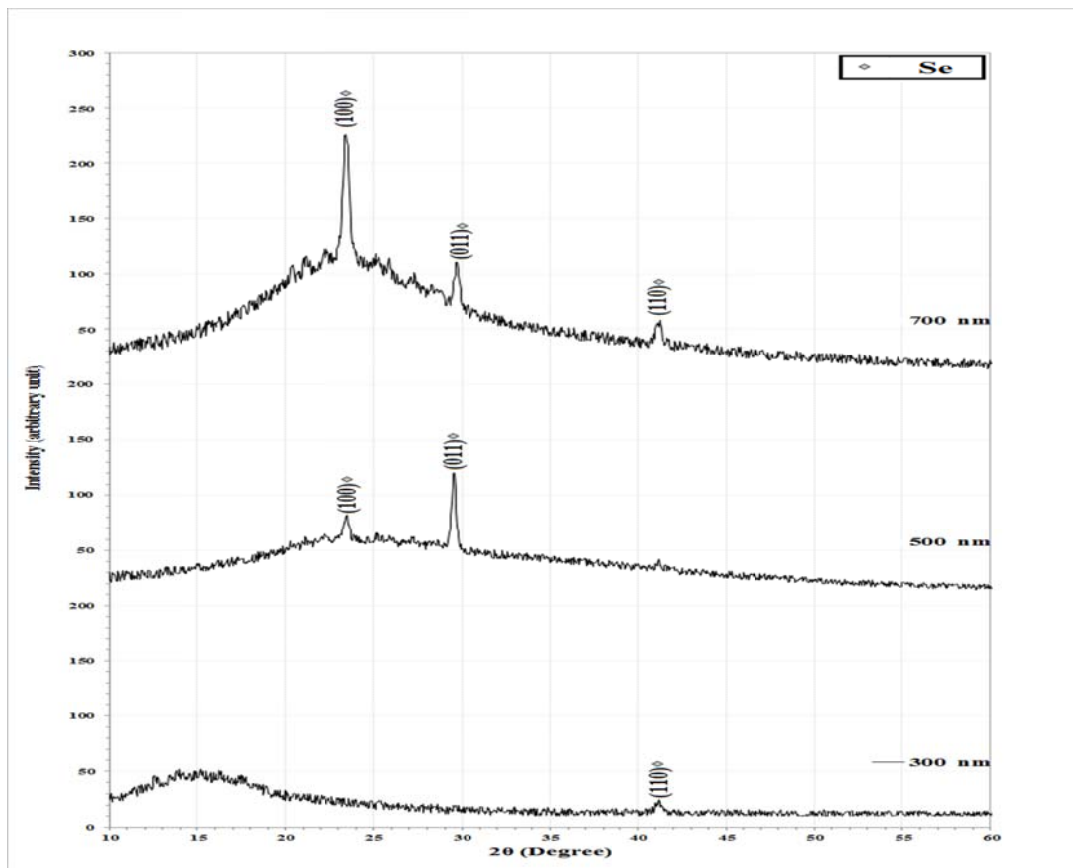


Fig. 2: X-ray diffraction patterns for  $\text{In}_{10}\text{Se}_{90}$  thin films at different thicknesses.

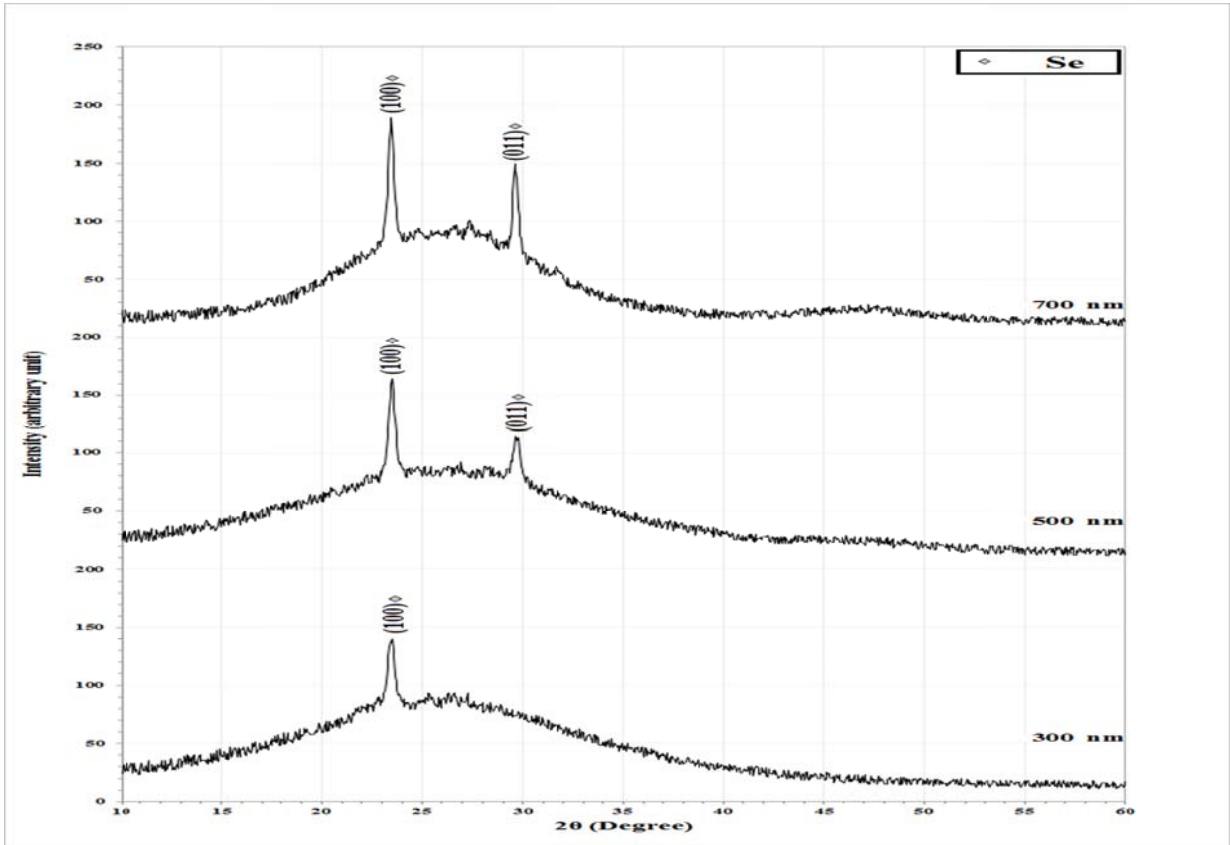


Fig.3: X-ray diffraction patterns for  $In_{20}:Se_{80}$  thin films at different thicknesses.

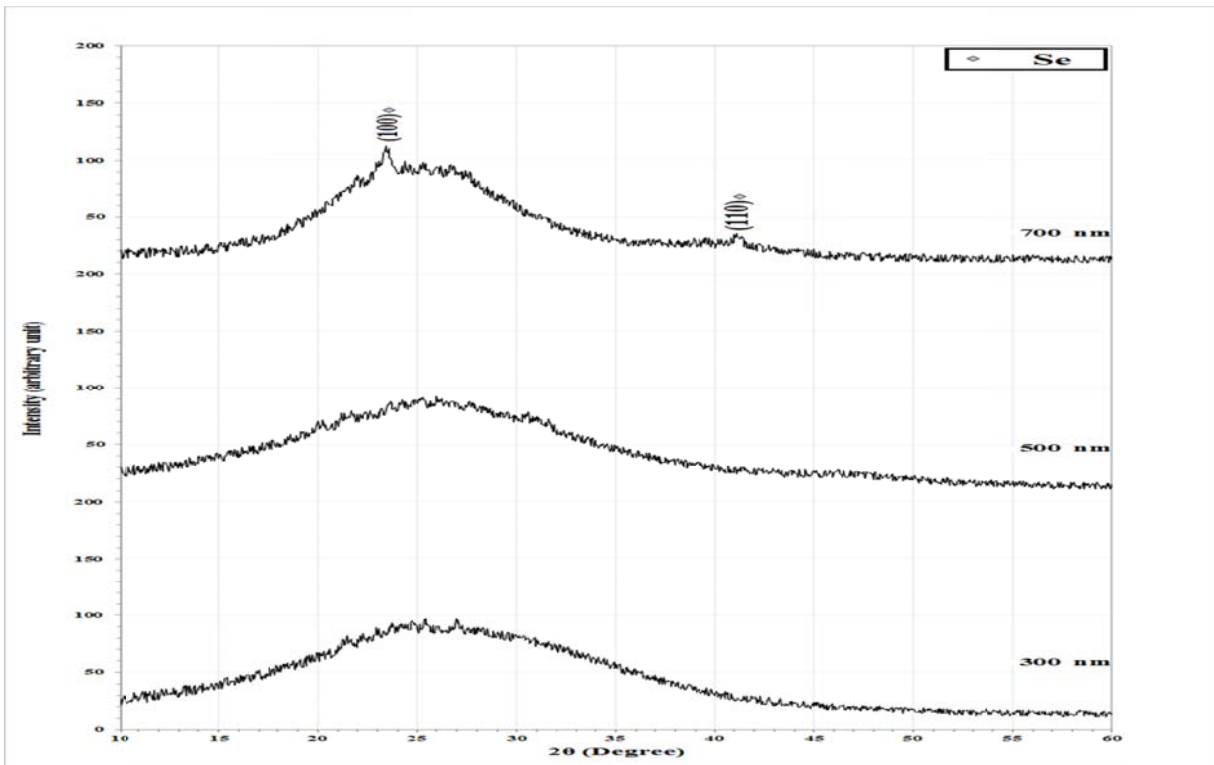
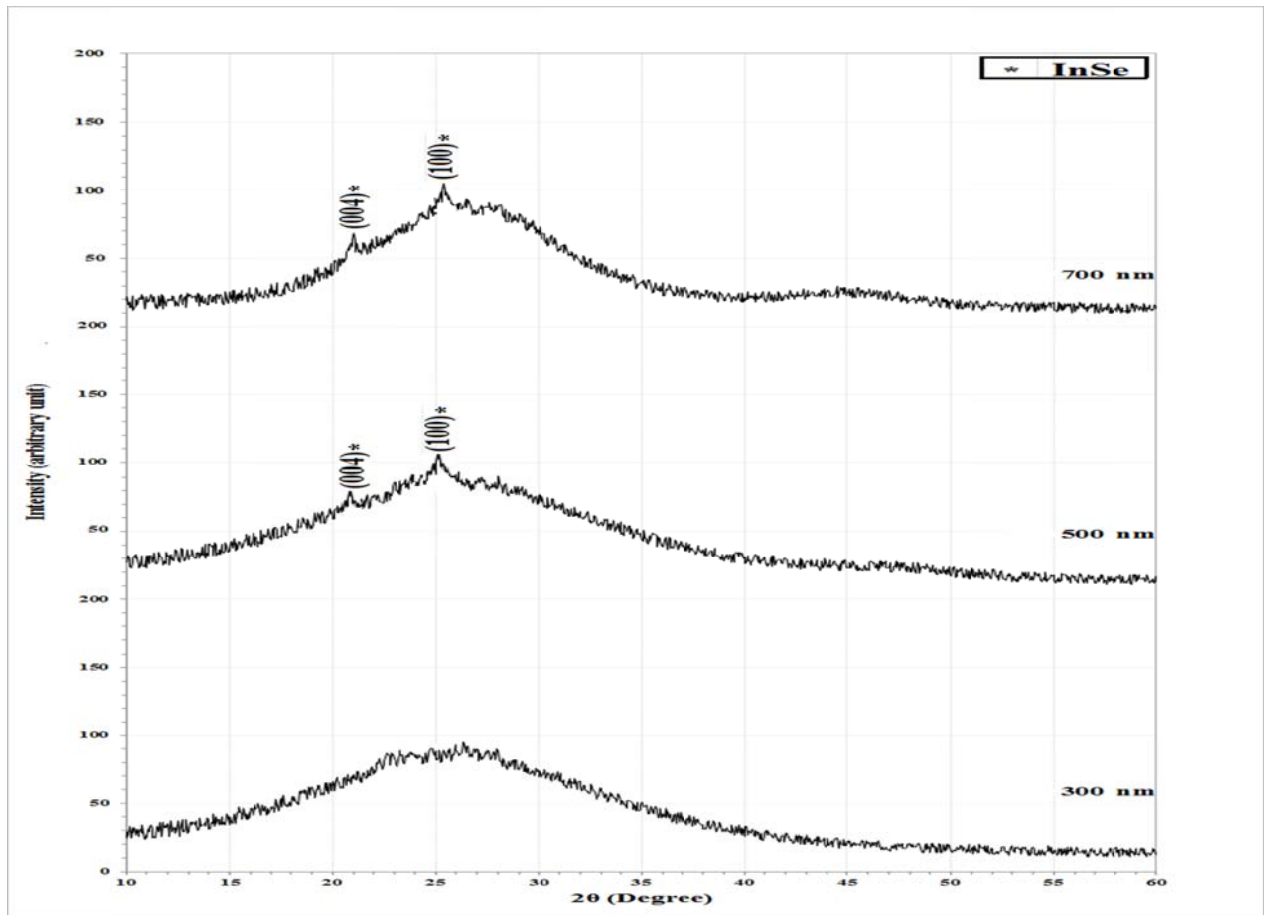


Fig.4: X-ray diffraction patterns for  $In_{30}:Se_{70}$  thin films at different thicknesses.



**Fig.5: X-ray diffraction patterns for  $In_{40}:Se_{60}$  thin films at different thicknesses.**

Table 2 shows all peaks observed in the X-ray pattern and those FWHM and grain size and the identical standard peaks from JCPDS. The results show that grain size increases with the increase of indium concentration at  $t=700$  nm in the first stage but the decreases with further increase of indium concentration, indeed the grain size increase from 21.6 to 23.6 nm when indium concentration increase from  $x=10$  to 30 but then decrease to 17.2 nm when indium concentration increase to  $x=30$ . the structure at  $x=40$  of  $In_xSe_{1-x}$  films is amorphous. The results lead to concludes that increase of indium enhance the structures up to  $x=20$  but

then decreases the degree of crystallinity throughout decreases the grain size of the films textures. The increase of thickness leads to enhanced the structure throughout transfer the structure from amorphous to polycrystalline, which reflects as appearing of small peaks located at  $2\theta=20.86^\circ$  and  $25.08^\circ$ , the further increase of thickness leads to little shift of  $2\theta$  to  $20.93^\circ$  and  $25.379^\circ$  as well as increase of grain size from 13.9nm to 22.2 nm of the plane of proffered growth (004). On the other hand increase of indium content lead to appear of InSe phase in addition of Se phase.

Table 2: Structural parameters for In:Se thin films at different ratio and different thicknesses.

In:Se	t (nm)	2 $\theta$ (Deg.)	FWHM (Deg.)	Int. (a.u)	d <sub>hkl</sub> Exp.(Å)	G.S (nm)	hkl	Phase	d <sub>hkl</sub> Std.(Å)	Card No.	
10:90	300	41.191	0.435	10	2.1898	19.5	(110)	Se	2.184	901-1649	
		23.460	0.376	20	3.7890	21.6	(100)	Se	3.7828	901-1649	
	700	29.520	0.282	70	3.0235	29.1	(011)	Se	3.0074	901-1649	
		23.460	0.376	118	3.7890	21.6	(100)	Se	3.7828	901-1649	
		29.700	0.376	39	3.0056	21.9	(011)	Se	3.0074	901-1649	
		41.180	0.400	20	2.1904	21.2	(110)	Se	2.1840	901-1649	
20:80	300	23.440	0.426	60	3.7890	21.6	(100)	Se	3.7828	901-1649	
		23.480	0.376	80	3.7858	21.6	(100)	Se	3.7828	901-1649	
	700	29.680	0.447	40	3.0076	18.4	(011)	Se	3.0074	901-1649	
		23.440	0.344	110	3.7922	23.6	(100)	Se	3.7828	901-1649	
		29.620	0.282	80	3.0135	29.2	(011)	Se	3.0074	901-1649	
		300	Amorphous								
30:70	500	Amorphous									
	700	23.440	0.471	25	3.7922	17.2	(100)	Se	3.7828	901-1649	
		41.182	0.465	8	2.1902	18.3	(011)	Se	3.0074	901-1649	
	40:60	300	Amorphous								
500		20.860	0.583	16	4.2550	13.9	(004)	InSe	4.2325	900-8968	
		25.087	0.802	21	3.5468	10.2	(100)	InSe	3.5074	900-8968	
700		20.933	0.364	18	4.2403	22.2	(004)	InSe	4.2325	900-8968	
		25.379	0.583	25	3.5067	14.0	(100)	InSe	3.5074	900-8968	

### Optical studies

The relation between  $(n^2-1)^{-1}$  and  $(h\nu)^2$  as shown in Fig.6 can be estimate many parameters like the values of the  $E_0$  which is an average energy gap  $E_0 \approx 2Eg$ , and  $E_d$  can be determined from the intercept  $E_0/E_d$  and the slope  $(E_0E_d)^{-1}$ . The values of dispersion parameters,  $E_0$ ,  $E_d$ , static refractive index, and static dielectric constant,  $\epsilon_s$  are listed in Table 3. The static refractive index and static dielectric constant were calculated were found to be 3.9 and 15.76, 2.94 and 8.45, 2.24 and 5.05, 2.85 and 8.13 for  $In_{10}Se_{90}$ ,  $In_{20}Se_{80}$ ,  $In_{30}Se_{70}$  and  $In_{40}Se_{60}$  respectively. Comparing the current calculated data with the previously published for the as grown sample [22,

23] as 2.97 and 25.05, 3.07 and 9.43 for  $In_{50}Se_{50}$ , is well coincide with these data.

It was observed that, the single oscillator energy  $E_0$  decreases while, both the dispersion energy  $E_d$  and  $n_0$  increases with the increase of In content. An important indication of the WDD model is that the relation between the dispersion energy,  $E_d$ , and other physical parameters of the material like the effective coordination number of the cation nearest-neighbor to the anion, the formal chemical valency of the anion, the effective number of valence electrons per anion. Thus to evaluate the compositional trended of  $E_d$  it is suitable to proposed

that, the observed decrease in  $E_d$  with increasing In content up  $x=30$  is primarily due to the change in the ionicities (homopolar Se–Se bonds are introduced together with extra Se atoms) [24], which decreases with

increasing the In content (see Table 3). The values of the single oscillator energy, the dispersion energy, the static refractive index for the  $In_xSe_{1-x}$  thin films are listed in Table 3.

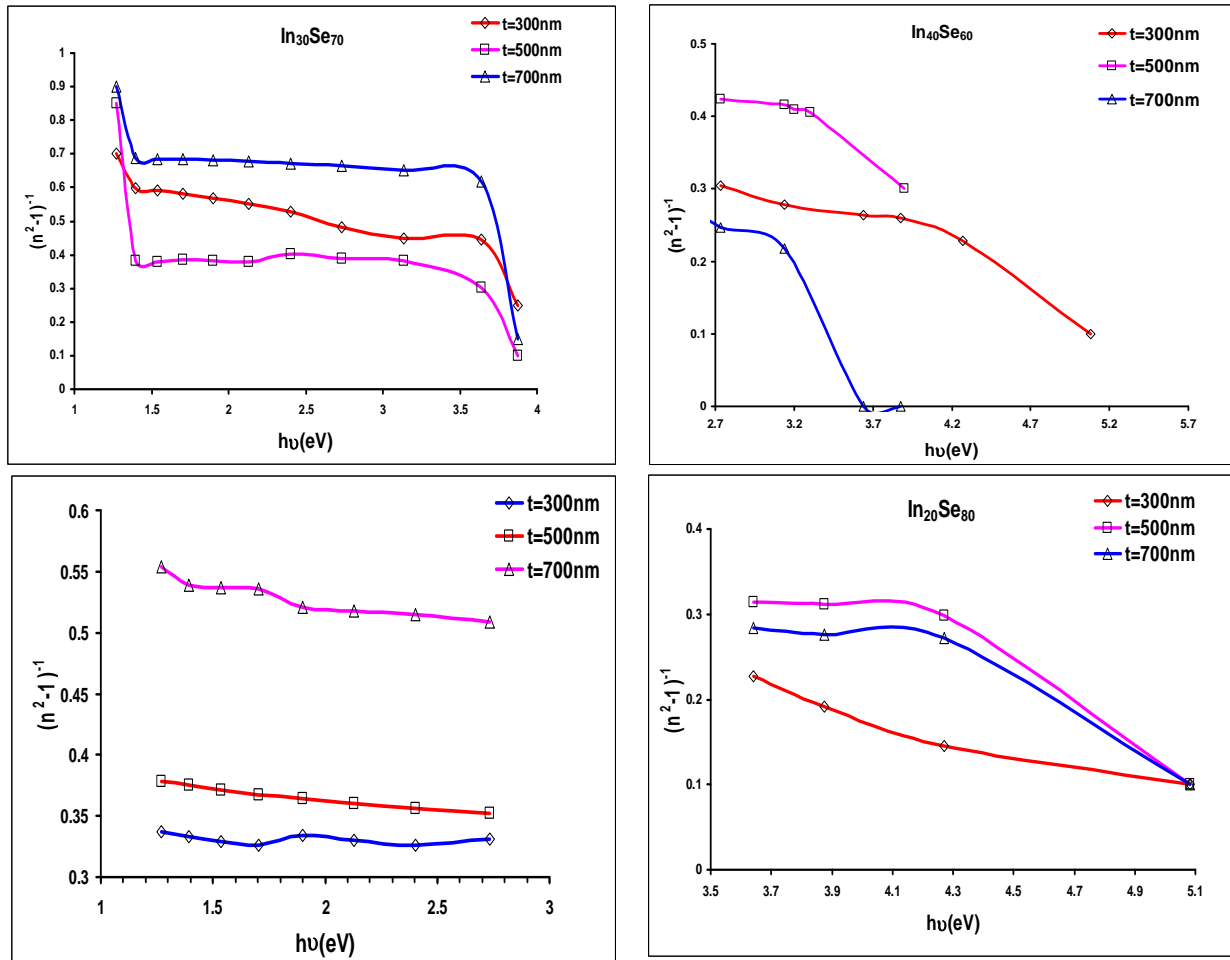


**Fig.6: Variation of  $(hv)^2$  with  $(n^2-1)^{-1}$  of  $In_xSe_{1-x}$  thin films with different indium content and different thicknesses.**

**Table 3: Value of  $E_d$ ,  $E_0$ ,  $n_0$ , and  $\epsilon_s$  of  $In_xSe_{1-x}$  thin films with different indium content and different thicknesses.**

Sample	t(nm)	$E_d$	$E_0$	$n_0$	$\epsilon_s=n_0^2$	$E_g=E_0/2$
$In_{10}Se_{90}$	300	928.1259	312.5	3.970003	15.76092	1.985001
	500	140.7662	56.17978	3.505638	12.2895	1.752819
	700	60.74555	35.33569	2.719099	7.3935	1.35955
$In_{20}Se_{80}$	300	22.44316	11.76471	2.907669	8.454538	5.882353
	500	9.801615	7.64526	2.282051	5.207758	3.82263
	700	7.137535	6.480881	2.101322	4.415552	3.240441
$In_{30}Se_{70}$	300	10.43937	8.368201	2.247505	5.051279	4.1841
	500	11.52557	7.936508	2.452222	6.013392	3.968254
	700	7.136804	6.978367	2.022704	4.091332	3.489184
$In_{40}Se_{60}$	300	22.89063	12.36094	2.851852	8.133059	1.425926
	500	11.79079	8.912656	2.322926	5.395987	1.161463
	700	5.212948	4.474273	2.165094	4.687631	1.082547

For all the prepared thin film samples, optical transmission was measured in the wavelength range 200–1100 nm. The optical constants are obtained by using only the transmission spectrum. For the method proposed by Swanepoel [25], the optical constants are deduced from the fringe patterns in the transmittance spectrum. The refractive index in the transmittance region where  $\alpha \approx 0$  was calculated by using the formula

$$n = \sqrt{N + \sqrt{N^2 - s^2}} \text{ where}$$

$$N = \frac{2S}{T_{\min}} - \frac{S^2 + 1}{2} \quad (3)$$

In the weak region where the absorption coefficient ( $\alpha \neq 0$ ) the value of N is given by

$$N = 2S \frac{T_{\max} - T_{\min}}{T_{\max} T_{\min}} + \frac{S^2 + 1}{2} \quad (4)$$

where  $T_{\max}$  is the upper extreme transmission point and  $T_{\min}$  lower extreme transmission point for particular wavelength and ‘s’ is the refractive index of the glass substrate ( $S = 1.5$ ). If  $n_1$  and  $n_2$  are the refractive indices of two adjacent maxima or minima at wavelengths  $\lambda_1$  and  $\lambda_2$ , then the thickness of the film is given by

$$d = \frac{\lambda_1 \lambda_2}{2(\lambda_1 n_2 - \lambda_2 n_1)} \quad (5)$$

The extinction coefficient k can be calculated from the following relation

$$k = \frac{\lambda}{4\pi d} \ln\left(\frac{1}{x}\right) \quad (6)$$

where x is the absorbance, given by

$$x = \frac{E_M - [E_M^2 - (n^2 - 1)^3(n^2 - s^4)]^{1/2}}{(n - 1)^3(n - s^2)} \quad (7)$$

and

$$E_M = \frac{8n^2 s}{T_M} + (n^2 - 1)(n^2 - s^2) \quad (8)$$

The absorption coefficient  $\alpha$  can be calculated from the relation given as:

$$\alpha = \frac{4\pi k}{\lambda} \quad (9)$$

The real and imaginary dielectric constant of amorphous thin films has been calculated by the relation (10) and (11), respectively.

$$\epsilon_r = n^2 - k^2 \quad (10)$$

and

$$\epsilon_i = 2nk \quad (11)$$

Fig.7 shows the transmittance spectra of  $\text{In}_x\text{Se}_{1-x}$  films for different In content and thicknesses (300, 500 and 700) nm. It is obvious that the transmittance of all deposited thin films increases with increasing of ( $\lambda$ ). On the other hand the transmittance decreases with the increase of In content and sample thickness which means increase in the reflection and absorption. The shifts of transmittance toward (lower energies) accompanied the thickness increment explained according to the fact that increasing of thickness approach the structure of samples from bulk material which indicated that absorption edge is shifted to the higher wavelengths with the increase of the thickness of the films and the effect of photo darkening is remarkable, while the decrease of transmittance with the increase of In content attributed to that the addition of In to Se increases the density and consequently the samples because more opaque to the incident light. It is clearly seen from transmittance spectra that in the weak absorption region, sharp interference fringes were apparent with increase of t indicated that the interfaces air/layer, and layer/glass were flat and parallel.

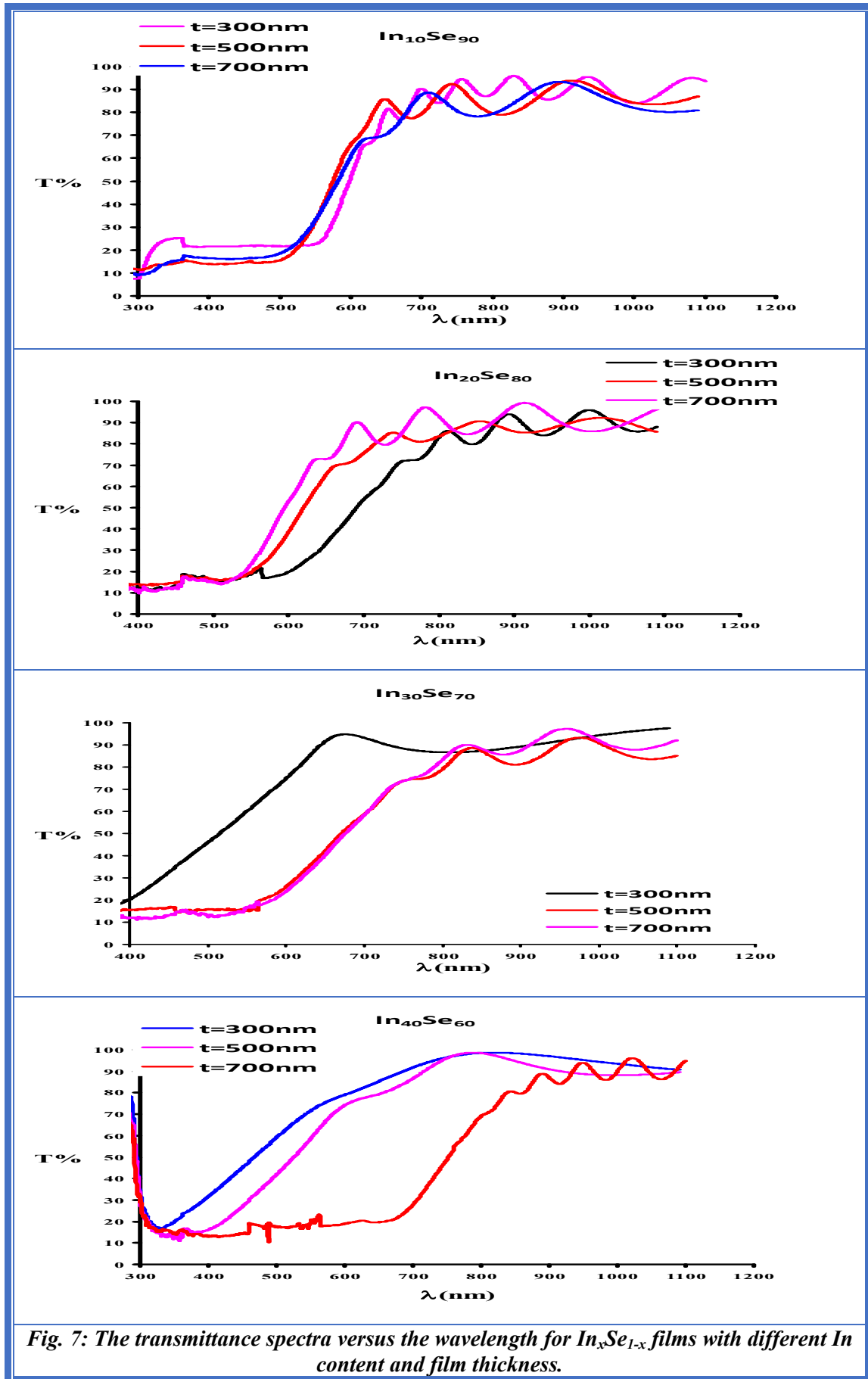


Fig. 7: The transmittance spectra versus the wavelength for  $In_xSe_{1-x}$  films with different In content and film thickness.

Strong absorption was observed at wavelengths lower than 700 nm, Moreover, the observed maxima and minima positions of the interference fringes in reflectance spectra at the same wavelength positions of the corresponding minima and maxima in transmittance spectra indicates the optical homogeneity of the deposited films. The refractive index of the deposited  $\text{In}_x\text{Se}_{1-x}$  films have been determined from the recorded transmission spectra using Swanoepl's method. The spectral distribution of refractive index ( $n$ ) and extinction coefficient ( $k$ ) for three thickness of the  $\text{In}_x\text{Se}_{1-x}$  system with wavelength is given in Figs. 8 and 9 respectively. From the Figs. 8 and 9 it is clear that both the refractive index and extinction coefficient decrease with the increase in the wavelength. It is clearly seen that dispersion in the values of refractive indices for different film thickness has been observed especially for higher wavelengths values, and the dispersion increases slightly at lower wavelength values. This result indicates that the refractive index is thickness dependent. It can be noticed from these figures and also from Table 4 that the refractive index, decreases with the increase of thickness for polycrystalline samples i.e. at  $x=10$  and  $20$ , while  $n$  increases with thickness for amorphous samples i.e. at  $x=30$  and  $40$ ; indeed  $n$  decreases from  $2.01653$  to  $1.71527$  and from  $1.90870$  to  $2.04516$  while  $n$  increases  $1.69944$  to  $2.12745$  and from  $1.57742$  to  $2.08590$ , when  $t$  increases from  $300$  to  $700\text{nm}$  at  $\lambda=800\text{nm}$ . This decrease of  $n$  attributed to decrease of localized states accompanied. structural enhancement while increase of  $n$  attributed to increase of absorbance related the amorphous state. On the other hand, the refractive index decreases with the increase of the In content up to  $30$  and then  $n$  get

increase with indium content, indeed( $n$ ) decreases from  $2.01653$  to  $1.69944$  and from  $1.95118$  to  $1.86899$  and from  $1.71527$  to  $1.71527$  when In content increases from  $10$  to  $30$  but then increase to  $2.12745$ ,  $1.84863$ ,  $2.08590$  when  $x=40$  for  $300$ ,  $500$  and  $700$  nm, respectively.

It can be observed from Fig. 8 and Table 4 that the extinction coefficient varies rapidly with the increase of In content and film thickness for all prepared samples. It is obvious that  $k$  decreases with increase of indium in first stage but then increases with further increase of indium. This is attributed to the same reason mentioned previously, since the increase of In content eliminate the defect states and increase grain size in the first but the then change the structure to amorphous, which in turn increases the absorbance of the material.

The variation of real  $\epsilon_r$  and imaginary  $\epsilon_i$  parts of the dielectric constant values with wavelength in the range of  $(300 - 1100)\text{nm}$  for  $\text{In}_x\text{Se}_{1-x}$  films deposited at different In contents ( $x = 10, 20, 30$  and  $40$ ) and thicknesses ( $t = 300, 500$  and  $700$  nm) are shown in Figs.10 and 11.

The behavior of  $\epsilon_r$  is similar to that of the refractive index because of the smaller value of  $k^2$  compared with  $n^2$  value according to Eq. (10), while  $\epsilon_i$  depends mainly on the  $k$  values according the Eq. (11). It is found that  $\epsilon_r$  changes with the increases of film thickness and In content. Moreover  $\epsilon_r$  found to decrease with thickness for polycrystalline samples i.e.  $x=10$  and  $20$ , while  $\epsilon_r$  tend to increase with thickness for amorphous samples i.e.  $x=30$  and  $40$ , as shown in Fig. 9 and Table 4.

The imaginary part of dielectric constant  $\epsilon_i$  reveals the same behavior of  $\epsilon_r$  with the variation of film thickness and In content. It is clear

from Fig.10 that  $\epsilon_i$  decreases with thickness for low indium content samples, but then increase for high

indium content samples as shown in Table 4. The same explanation of  $n$  and  $k$  can be given to  $\epsilon_r$  and  $\epsilon_i$ .

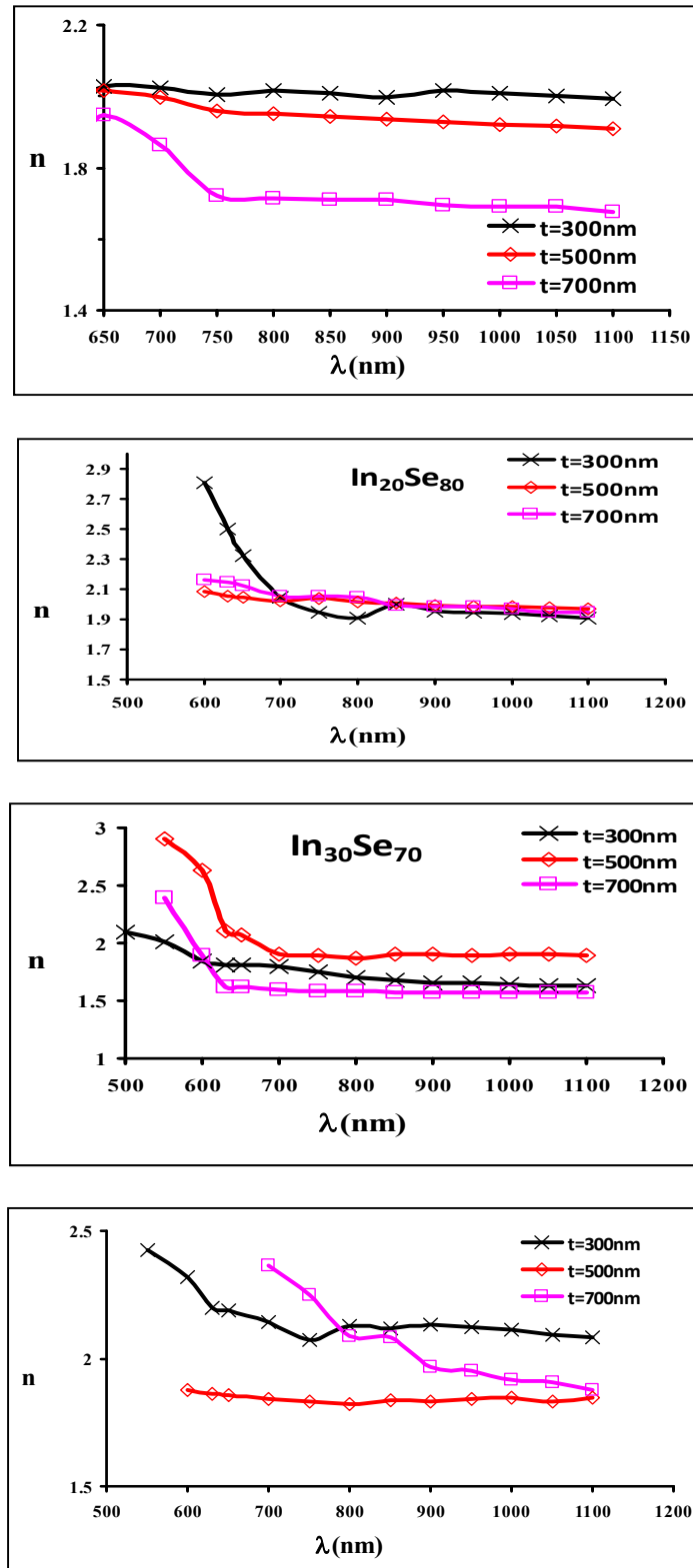


Fig. 8: Variation of refractive index with the wavelength for  $In_xSe_{1-x}$  films with different In content and film thickness.

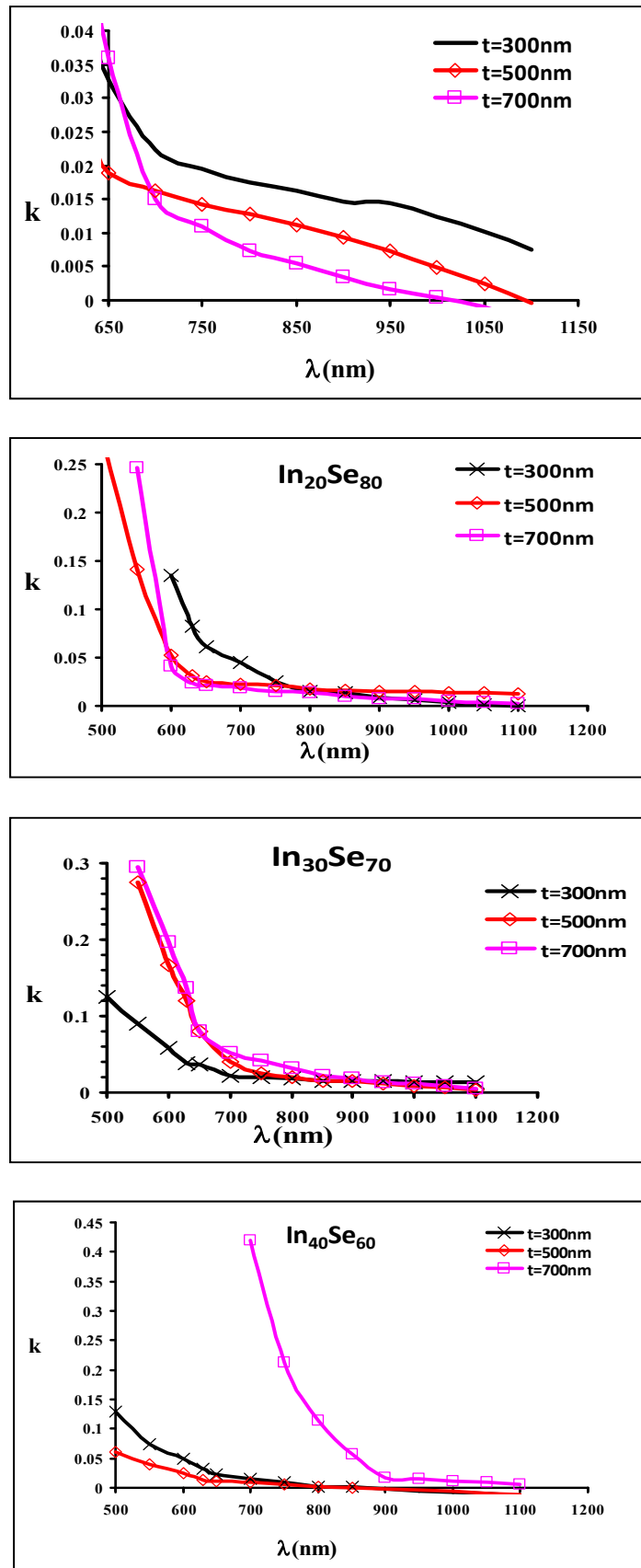


Fig. 9: Variation of extinction coefficient  $k$  with wavelength for  $In_xSe_{1-x}$  films with different In content and film thickness.

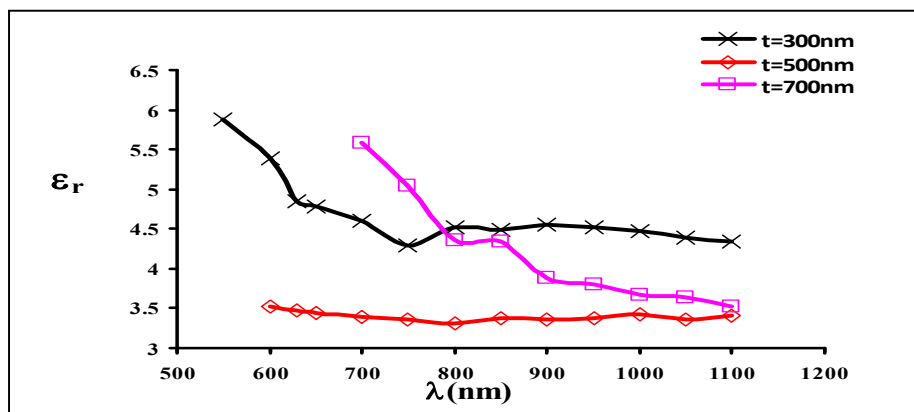
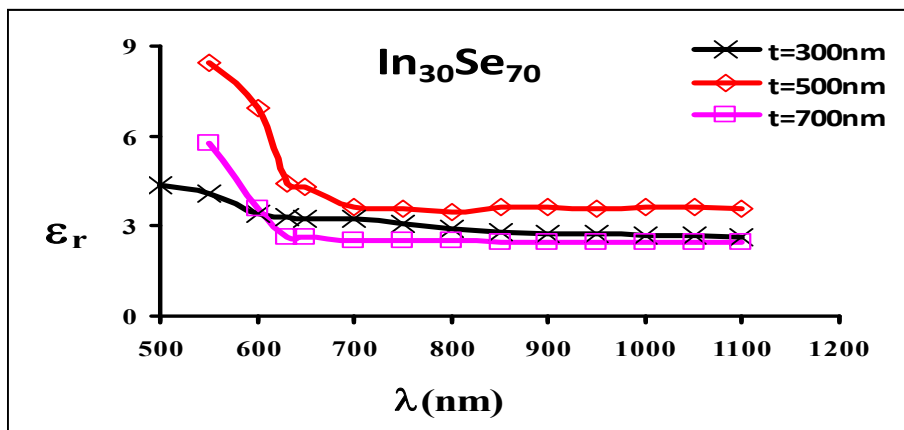
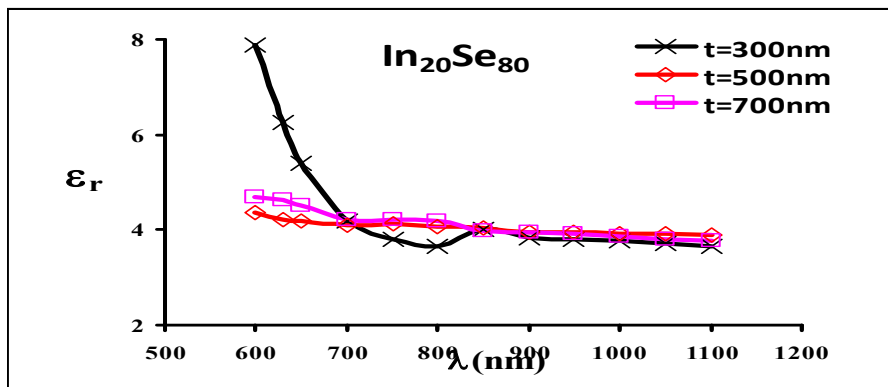
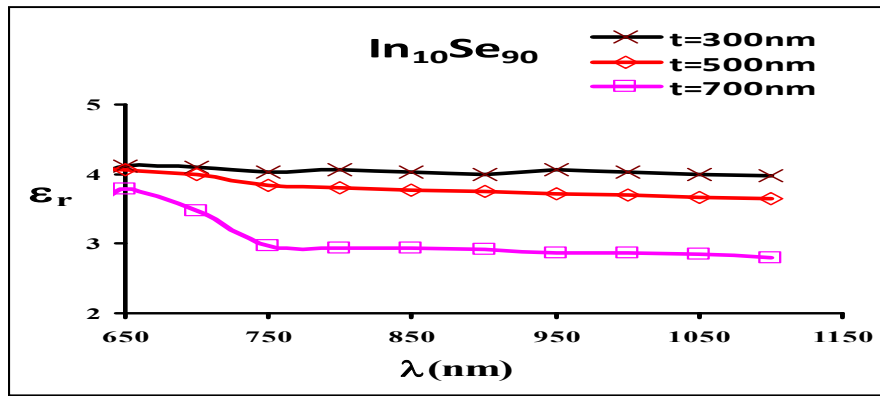
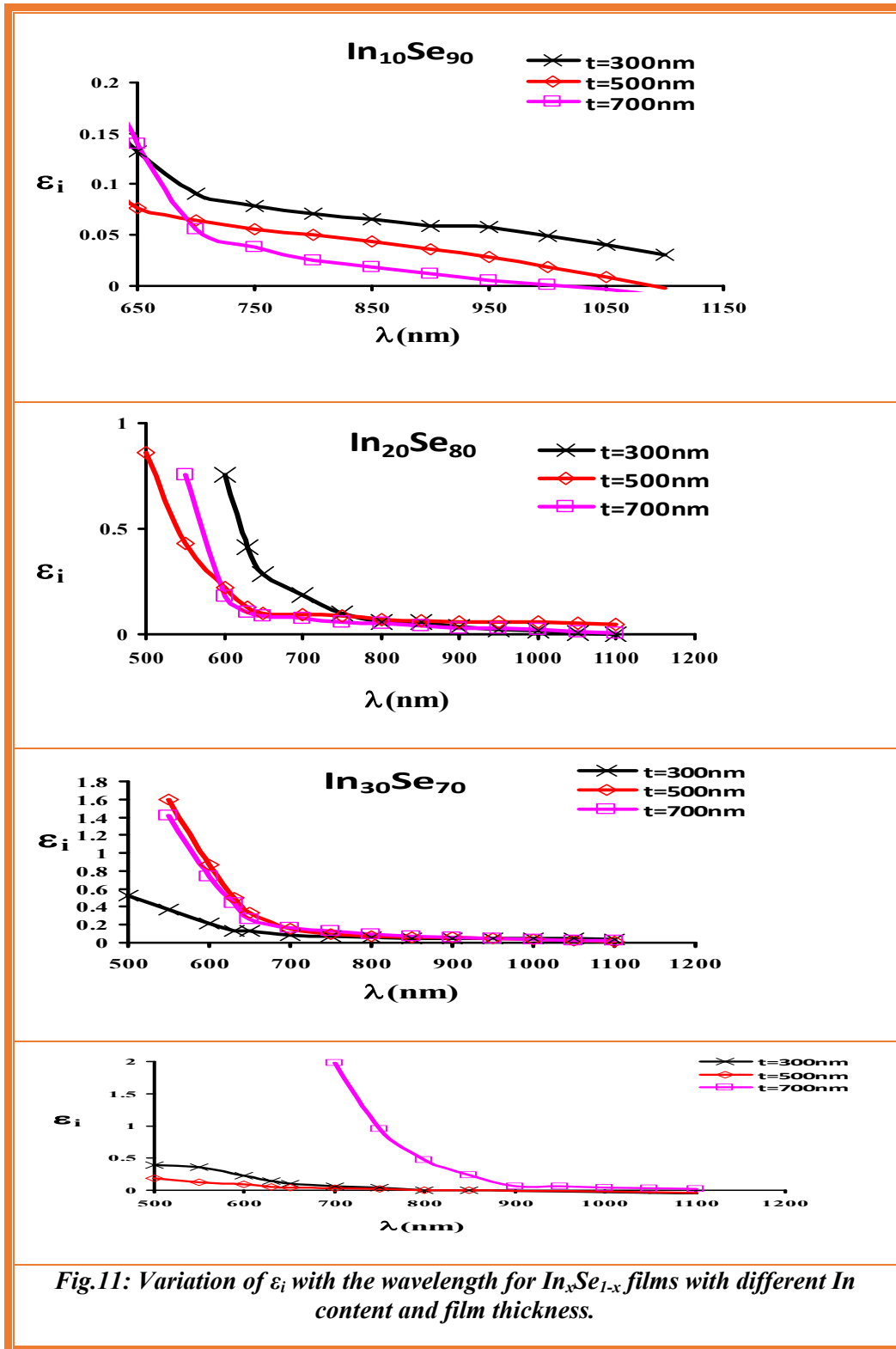


Fig.10: Variation of  $\epsilon_r$  with the wavelength for  $In_xSe_{1-x}$  films with different In content and film thickness.



**Table 4: Illustrate the values of optical constants at  $\lambda=800$  nm for  $In_xSe_{1-x}$  films with different In content and thicknesses.**

t (nm)	x	T%	k	n	$\epsilon_r$	$\epsilon_i$
300	10	0.84247	0.01755	2.0165	4.066	0.07081
	20	0.85581	0.01487	1.9087	3.643	0.056784
	30	0.84690	0.01766	1.6994	2.888	0.060029
	40	0.91828	0.00096	2.1274	4.526	0.004125
500	10	0.86436	0.01279	1.9511	3.807	0.049934
	20	0.84247	0.01755	2.0165	4.066	0.07081
	30	0.83702	0.01941	1.8689	3.493	0.072582
	40	0.91169	0.00246	1.8486	3.417	0.009115
700	10	0.92903	-0.00131	1.7152	2.942	-0.0045
	20	0.86069	0.01334	2.0451	4.182	0.054588
	30	0.79496	0.03129	1.5774	2.488	0.098731
	40	0.51262	0.11393	2.0859	4.350	0.475299

### References

- [1] T.Matsushita, T.T.Nang, M.Okuda, A.Suzuki, S.Yokota, Jap. J. Appl. Phys., 15 (1976) 901.
- [2] T.T.Nang, T.Matsushita, M.Okuda, A.Suzuki, Jap. J. Appl. Phys., 16 (1977) 253.
- [3] A.Segura, J.M.Besson, A.Chevy, M.S.Martin, Nuovo Cimento, 38B (1977) 345.
- [4] C.Cleman, X.I.Saldana, P.Munz, E.Bucher, Phys. Stat. Solidi (a), 49 (1978) 437.
- [5] V.L.Bakumenko, Z.D.Kovalyuk, L.N.Kurbatov, V.F.Chishko, Sov.Phys. Semicond., 12 (1978) 1307.
- [6] A.Segura, J.P.Guesdon, J.M.Besson, A.Chevy, Rev.Phys.Appl, 14 (1979) 253.
- [7] K.Ando and A.Katsui, Thin Solid Films, 76 (1981) 141.
- [8] Y.Hasegawa and Y.Abe, Phys.Stat. Solidi(a), 70 (1982) 615.
- [9] T.Matsushita, A.Suzuki, M.Okuda, H.Naitoh, T.Nakau, Jap. J. Appl. Phys., 22 (1983) 762.
- [10] A.Segura, J.P.Guesdon, J.M.Besson, A.Chevy, J. Appl. Phys., 54 (1983) 876.
- [11] A.Segura, J.L.Valdes, F.Pomer, A.Cantarero, A.Chevy, in Proc.5th' E.C.Photovolt. Sol. Energy Conf., Kavouri, 1983 (Reidel, Dordrecht, 1984), p.927.
- [12] J.L.Valdes, A.Cantarero, F.Pomer, J.P.Martinez, A.Sugura, B.Mari, A.Chevy, in: Proc. Euro. Communities Photovolt. Sol. Energy Conf., Londres, 1985 (Reidel, Dordrecht, 1985), p.774.

- [13] J.Martinez-Pastor, A.Segura, J.L.Valdes, A.Chevy, *J. Appl. Phys.*, 62 (1987) 1477.
- [14] S.Shigetomi, T.Ikari, Y.Koga, S.Shigetomi, *Jap. J. Appl. Phys.*, 27 (1988) 1271.
- [15] J. Hossain, M. Julkarnain, K. S. Sharif, K. A. Khan, *International Journal of Renewable Energy Technology Research*, 2, 9, September (2013) 220 – 226.
- [16] J. F. Sa´nchez-Royoa, A. Segura, O. Lang, E. Schaar, C. Pettenkofer, W. Jaegermann, W. Jaegermann, *Journal of Applied Physics*, 90, 6 (2001)2818.
- [17] K. Ando and A. Katsui. *Thin Solid Films*,76 (1981) 141.
- [18] J.Cheon, J.Arnold, K.M. Yu, E.D. Bourret, *Chem. Mater*, 7,12 (1995) 2273–2276.
- [19] M.Emziane, R. Le Ny, *J. Phys. D. Appl. Phys.* 32 (1999) 1319.
- [20] Amar H. Jareeze, *Journal of Al-Nahrain University*, 16, 2 July (2013) 124-128.
- [21] J. Hossain, Md. Julkarnain, K. Shaifullah Sharif, K. Alam Khan, *Journal of Physical Science and Application*, 1 (2011) 37-43.
- [22] S. H. Wemple, M. DiDomenico, *Phys. Rev.*, B 3 (1971) 1338.
- [23] A. F. Qasrawi, *Optical Materials*, 29 (2007) 1751.
- [24] H. Bouzouita, N. Bouguila, S. Duchemin, S. Fiechter, A. Dhouib, *Renewable Energy*, 25 (2002) 131.
- [25] R. Swanepoel, *J. Phys. E: Sci. Instrum.*, 16 (1983) 1214.